

The fault in our sirens: Hierarchical diagnosis of waveform systematics in Hubble-Lemaître-constant measurements

Arnab Dhani ^{1,*}, Jonathan Gair ¹ and Alessandra Buonanno ^{1,2}

¹*Max Planck Institute for Gravitational Physics (Albert Einstein Institute), Am Mühlenberg 1, Potsdam 14476, Germany*

²*Department of Physics, University of Maryland, College Park, MD 20742, USA*

Cosmological inference using a population of binary black-hole mergers, combined with a galaxy catalog, presents an exciting opportunity for precision cosmology with the possibility of resolving the Hubble tension. However, the accuracy of these measurements heavily relies on the quality of the model used to infer the binary parameters, including the model of the gravitational-wave signal. We use state-of-the-art waveform models to explore the impact of inaccurate modeling in measuring the Hubble-Lemaître constant for the upcoming and future ground-based gravitational-wave observatories. We diagnose the presence of inaccuracies within a hierarchical population-analysis framework, without a priori knowing the true value of the parameter, by assessing the consistency of the distribution of individual posteriors in relation to their measurement errors. Our findings indicate that even a small high-mass, spin-precessing subpopulation—comprising as little as 5% of the population generating the events observed by the LIGO-Virgo-KAGRA Collaboration so far—can result in an unreliable measurement of the Hubble-Lemaître constant in the upcoming observing runs of these detectors, with even more pronounced effects expected in future facilities on the ground.

Introduction— Gravitational-wave (GW) cosmology has emerged as a promising independent method for probing the cosmic expansion history of the Universe [1, 2]. GWs from compact-binary coalescences (CBCs) serve as standard sirens that measure distance without relying on the traditional cosmic distance ladder. When combined with redshift measurements, these distances can be used to estimate various cosmological parameters [3]. Several methods exist to obtain the redshift information of a GW event. The most straightforward approach is when an identifiable electromagnetic (EM) counterpart localizes the host galaxy of the GW event, as demonstrated for GW170817 [4]. However, most GW events do not have an associated EM counterpart. In such cases, a statistical measurement of the Hubble-Lemaître parameter (H_0) can be obtained using a galaxy catalog of probable hosts, either by directly using the measured galaxy redshifts as a prior on the GW source redshifts [3, 5, 6], or by cross-correlation the inferred statistical distribution of galaxies and that of GW sources [7, 8]. Alternatively, redshift measurements can be obtained by examining the features in the mass, and indirectly the spin, distributions of the CBC population [9–13], or analyzing the stochastic GW background [14]. Additionally, tidal measurements from a binary neutron star (BNS) merger can provide the redshift to such GW sources [15–18].

With close to 100 observations of CBCs to date, the current estimate of H_0 using GWs is $H_0 = 68^{+8}_{-6} \text{ km s}^{-1} \text{ Mpc}^{-1}$ [2]. The ongoing observing run (O4) of the LIGO-Virgo-KAGRA (LVK) Collaboration [19–21] has already detected >200 signal candidates, and this number is expected to grow to thousands as the detectors reach their design sensitivity by the end of

the decade [22]. Additionally, proposed future detectors, like the Cosmic Explorer (CE) [23–25] and the Einstein Telescope (ET) [26–28], are anticipated to detect every stellar-origin binary black hole (BBH) merger in the Universe and every BNS merger up to a redshift of 1, increasing the observed population of CBCs to hundreds of thousands [22]. Since the measurement precision improves as the inverse square root of the number of observations, H_0 measurements using GWs could achieve sub-percent precision [6, 18, 29], positioning GW cosmology firmly in the realm of precision cosmology [30, 31].

Given the expected precision of these measurements, it is essential that they are also accurate. Accurate measurements are particularly critical because GW measurements aim to resolve the $\sim 5\sigma$ discrepancy in H_0 estimated in the local-Universe and in the pre-recombination era [30, 31].

Accurate waveform models are essential for an unbiased inference of a GW source’s binary parameters. Thanks to the advancements in GW modeling techniques, current state-of-the-art waveform models can effectively analyze most signals found in the LVK Gravitational-Wave Transient Catalogs (GWTCs) [32]. However, as detector sensitivities continue to increase, the accuracy of these waveform models will be challenged, particularly for binaries with large masses, asymmetries, and spins [33, 34]. Consequently, any systematic errors in the waveform models would affect the inference of the properties of the BBH population and likely impact the estimation of H_0 [33, 35].

While a direct EM counterpart accompanying a GW event would provide the most accurate measurement of H_0 , such events are infrequent; to date, only one has been observed [1, 36]. Therefore, “dark sirens” consisting of loud BBH mergers with no EM counterpart are expected to yield the most precise measurements, as there are likely to be few probable host galaxies within the lo-

* arnab.dhani@aei.mpg.de

calization volume [6, 29]. Previous studies of this method have focused on how assumptions regarding the population model and galaxy weights affect the measurement accuracies [2, 37]. However, none has systematically investigated the impact of inaccurate waveform models on the measurement of H_0 with this method.

In this *Letter*, we analyze the impact of inaccurate waveform models on the H_0 measurement using a population of simulated BBH mergers and host galaxies observed in current and future ground-based GW detectors. The current estimates from GWTC-3 indicate that most merging BBHs have relatively low masses, ranging from 10 to $30M_\odot$, exhibit small asymmetries, and have small spins with minimal, if any, spin-precession [38]. However, there are outliers, such as GW190521_030229 [39] and the candidate events GW190403_051519 and GW200208_222617 [40], that display larger masses, greater asymmetries, or higher spins, or some combination of these. While, the latter two events represent marginal detections with moderate astrophysical significance, the scientific potential of these events is substantial. Confident detections of similar events in the future will be invaluable and there are reasons to expect these to be observed. Although the current set of GW observations does not definitively demonstrate that black hole (BH) masses evolve with redshift [41, 42], astrophysical considerations tend to support the idea that they should [43–45], with larger masses, greater asymmetries, and higher spins expected at larger redshifts [46–48]. Moreover, strong lensing of GWs is expected to shift heavy systems at higher redshifts, nominally outside the detector horizon, into the detectable range. Unfortunately, these scientifically exciting systems are more challenging to model because numerical relativity (NR) simulations in these regions of the parameter space are limited. Consequently, significant systematic biases can arise when analyzing these systems [33, 35]. For this reason, it is vital to take into account the effect of unobserved, yet anticipated, populations of BHs when evaluating the impact of inaccurate waveform models on GW science and assessing the accuracy requirements for future waveform models. In this study, we embellish the population of BBH mergers as observed by the LVK Collaboration by including a small fraction of binaries with large masses, high asymmetries, and rapid spins.

H_0 is not a direct GW observable, but, rather, a characteristic of the population of GW sources. Therefore, a hierarchical Bayesian inference method is used to infer it from a distribution of sources. In an unbiased hierarchical inference, the individual H_0 posteriors should be distributed around the true value according to the noise properties. This is similar to how the posteriors on the parameters of individual GW events fluctuate around the true value for different noise realizations. However, when systematic biases are present — such as an incorrect noise model or waveform model — the consistency between the distribution of the individual posteriors

and the noise properties may not hold. Indeed, the probability-probability (P-P) plot is widely used in GW astronomy [49] to assess this consistency for the parameters of individual sources. Hanselman *et al.* [37] developed a diagnostic tool to utilize this consistency condition for population parameters by going a layer deeper in the hierarchical analysis, treating the individual H_0 posteriors as coming from a population. For Gaussian-distributed posteriors on the parameters of individual events whose values are themselves drawn from a normally distributed population model, the joint constraint on the mean converges to the mean of the population, with an uncertainty that depends on both the individual event uncertainties and the variance in the population. Differences between the population variance and the individual event uncertainties are then indicative of the spread of parameter values in the population. Applying this approach to a parameter that should be common to all events is a powerful method for identifying systematic biases because it is constructed within the analysis framework, eliminating the need for comparisons that involve different models and assumptions. We employ this method to detect systematic biases that arise from inaccurate waveform models. We find that the method is able to detect the presence of systematic biases, even in situations in which the joint posterior converges to the true value (which would in any case not be known a priori).

Diagnosing population systematics — We briefly formulate the method for identifying systematic biases introduced in Hanselman *et al.* [37] in a simplified setting. While the simplifications allow us to obtain simple analytical results, the observations remain valid even in the general case. Let us assume we have N noisy measurements of a parameter λ obtained from data \mathcal{D} . This gives us a set of likelihoods represented as $\{p(\mathcal{D}_i|\lambda^i)\}_{i=1}^N$. We will assume that each λ is drawn from a population characterized by a Normal distribution, $p(\lambda|\mu, \sigma) \sim \mathcal{N}(\mu, \sigma^2)$ where μ is the mean and σ^2 is the variance. In the hierarchical Bayesian inference framework, the likelihood function on $\{\mu, \sigma\}$ is given by

$$p(\{\mathcal{D}_i\}|\mu, \sigma) = \prod_{i=1}^N \int d\lambda^i p(\mathcal{D}_i|\lambda^i) p(\lambda^i|\mu, \sigma). \quad (1)$$

To understand the structure of the distribution mentioned above, it is useful to evaluate the maximum likelihood estimator. Assuming that the λ measurements are normally distributed with mean $\hat{\lambda}^i$ and variance σ_i^2 (i.e., $p(\mathcal{D}_i|\lambda^i) \sim \mathcal{N}(\hat{\lambda}^i, \sigma_i^2)$), the maximum likelihood estimates for $\{\mu, \sigma\}$, denoted by $\{\hat{\mu}, \hat{\sigma}\}$, is given by the solution of the following set of coupled equations [50]

$$\begin{aligned} \hat{\mu} &= \frac{\sum_{i=1}^N w_i \hat{\lambda}^i}{\sum_{i=1}^N w_i}, \\ \sum_{i=1}^N w_i - \sum_{i=1}^N w_i^2 (\hat{\lambda}^i - \hat{\mu})^2 &= 0, \end{aligned} \quad (2)$$

where, $w_i = 1/(\sigma_i^2 + \hat{\sigma}^2)$. There are no closed-form solutions to this set of equations. Therefore, under the simplifying assumption that the errors in all the individual observations of λ are the same, $\sigma_i = \sigma_\lambda$, we find

$$\begin{aligned}\hat{\mu} &= \frac{1}{N} \sum_{i=1}^N \hat{\lambda}^i \\ \hat{\sigma}^2 &= \frac{1}{N} \sum_{i=1}^N (\hat{\lambda}^i - \hat{\mu})^2 - \sigma_\lambda^2.\end{aligned}\quad (3)$$

In particular, Eq. (3) indicates that the maximum likelihood estimate of the population mean is the average of the individual observation means. It further states that the population variance is the difference the scatter of the individual posteriors ($\sum_{i=1}^N (\hat{\lambda}^i - \hat{\mu})^2 / N$) and the variance of the measurements (σ_λ^2).

Suppose the true population follows a δ -function, i.e., λ is common across all observations, then $\sigma \rightarrow 0$ by construction. This is the case for H_0 since it is a constant of nature. In this case, Eq. (3) asserts that $\hat{\sigma}$, on average, should be 0, and the scatter of the individual observations follows the measurement uncertainties. On the other hand, if σ is measured to be non-zero, this indicates the presence of systematic bias in the computation of H_0 . In a hierarchical Bayesian analysis, if the likelihood does not follow the true data-generating process — whether due to inaccuracies in the model, assumptions about the population, or characteristics of the noise — the posterior parameters will not only converge to a biased value as the number of observations increase, but the scatter of the individual observations will also be inconsistent with the assumed noise properties. While the first of these cannot be used as a diagnostic, since the true values of the parameters of interest are not known a priori, the scatter of the individual posteriors can serve as a diagnostic of model inconsistency. This is the key role of σ in Eq. (1). However, it is important to note that the source of the systematic error cannot be isolated. For instance, in this study, we examine systematic biases due to inaccurate waveform models, while Hanselman *et al.* [37] explored systematic biases due to inaccurate galaxy weights. We illustrate this in Fig. 1 where it is clear that in the absence of systematic biases due to inaccurate waveform models, the H_0 posteriors cluster around the injected value of $70 \text{ km s}^{-1} \text{ Mpc}^{-1}$ with a spread typical of the widths of the posteriors. In contrast, the posteriors affected by systematic biases are scattered randomly across the domain. Fig. 1 also illustrates the practical difficulty in combining the posteriors in the presence of systematic biases where the product of two narrow and separated PDFs can be zero at machine precision using floating point arithmetic. However, this issue is mitigated by treating the H_0 values as arising from a population as is done in this paper because we are no longer enforcing consistency in the means of the posteriors. We observe that, even when the models used for data generation and for the analysis are consistent, there are rare instances in

which the primary mode of the posterior is significantly separated from the true value. However, when this happens there is always a secondary mode that aligns with the true value. This is not unexpected, as galaxies or galaxy clusters are likely to be found within the localization volume, even if they did not host the GW event.

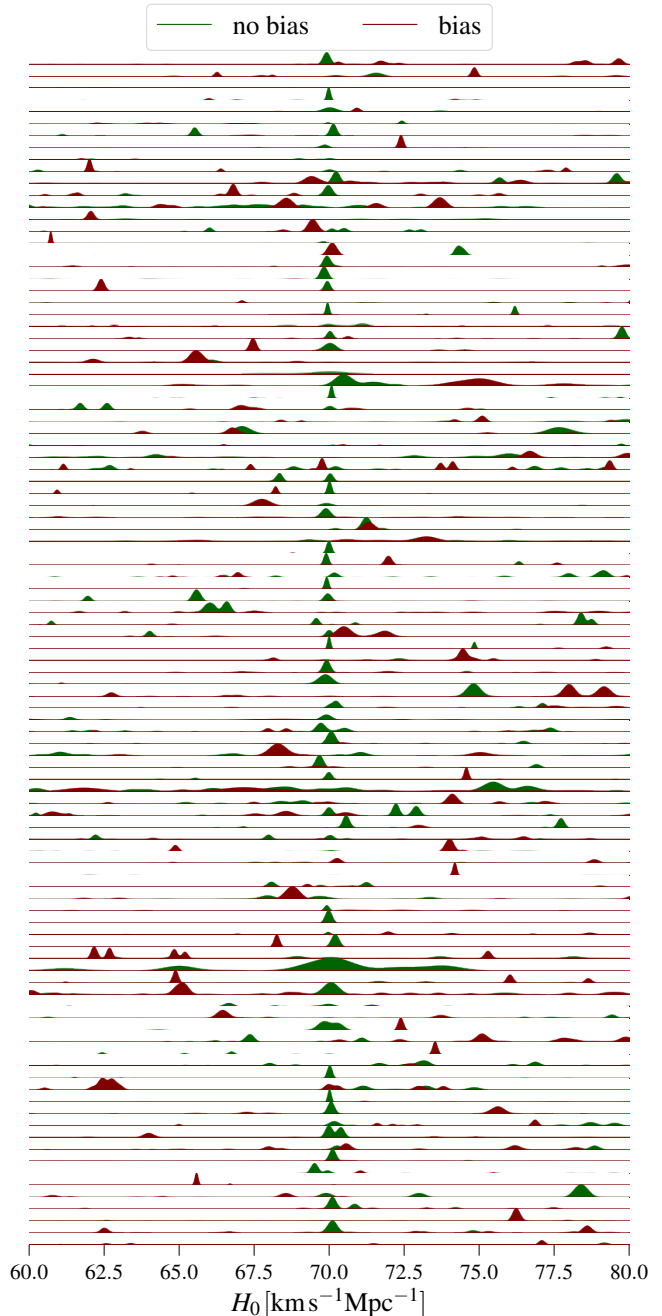


FIG. 1. The individual H_0 posteriors in the absence (green) and presence (red) of systematic bias of a random selection of 100 events with $\text{SNR} > 600$ for the high-mass spin-precessing population. It also illustrates the practical difficulty in combining the posteriors in the presence of systematic biases. The product of two narrow PDFs can be zero at machine precision using floating point arithmetic.

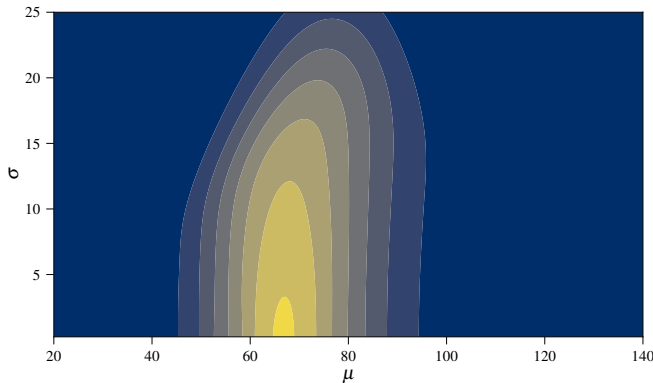


FIG. 2. The posterior distribution of the hyperparameters $\{\mu, \sigma\}$ for the real events used in the GWTC-3 cosmology paper.

We apply the hierarchical framework on the 46 real events used in Abbott *et al.* [2]. We use the publicly available H_0 posteriors of each event for our analysis. We choose the specific case corresponding to Fig. 7 of Abbott *et al.* [2]. The 2D posterior on $\{\mu, \sigma\}$ is shown in Fig. 2. We find that σ is consistent with zero and, therefore, the H_0 inference is not obviously affected by systematic biases. We confirm this observation for other population and galaxy catalog choices that were considered in Abbott *et al.* [2] and for which individual event posteriors are publicly available. While the contours move around on the μ axis signifying that the particular choices affect the measurement, as seen in Fig. 11 of Abbott *et al.* [2], we find that σ is consistent with zero in all the cases indicating that the distribution of the individual event posteriors is consistent with the assumptions of the models. We emphasize that, for these real events, the σ parameter is a test for any kind of systematics in the H_0 hierarchical likelihood and is not restricted to waveform systematics alone.

Systematic biases in upcoming observations— The current GW observations do not exhibit any systematic biases in the inference of H_0 . Therefore, we investigate the potential impact of systematic biases in both planned and future ground-based GW observatories. We simulate GW observations across three detector networks. These are (i) the O5 network, which consists of the two LIGO detectors and the Virgo detector, all operating at their design sensitivity; (ii) the A# network where the LIGO detectors operating at an upgraded A# sensitivity, while the Virgo detector continues to operate at design sensitivity; and (iii) the XG network made up of two CE detectors with arm lengths of 40 km and 20 km, along with a triangular ET with an arm length of 10 km. These networks represent highly probable observing scenarios for the future. The O5 network is expected to operate until the end of this decade, while the A# network is anticipated to begin functioning in the early part of the next decade, and the XG network is expected to be operational in the latter half of that decade.

We simulate a population of BBH mergers whose mass and spin distributions follow the median estimates from GWTC-3 [38, 40]. We embellish this population with varying fractions of a high-mass spin-precessing subpopulation (see Appendix B for details). We note that the fractions reported in this paper correspond to the full population and not the detected population. The corresponding fractions in the detected population depend on the signal-to-noise ratio (SNR) threshold and are impacted by the selection bias.

We assume that the redshift distribution of the GW sources follows the distribution of galaxies. To assign host galaxies and their corresponding redshifts and sky locations, we randomly select from the MICECAT mock galaxy catalog, which is complete and extends to a redshift of 1.4. We simulate a population of 100,000 binaries which correspond to a 4-yr observational period based on the estimates of the current merger rates [22, 38]. We apply a network SNR threshold of 70, 100, 600 for the three detector networks O5, A#, and XG, respectively. We chose these high SNR cutoffs to ensure that the GW detection horizon remains within that of the galaxy catalog. This is crucial to prevent the edge of the galaxy catalog — which contains information about H_0 — from skewing our estimates, as it could result in artificially lower error estimates for H_0 . Additionally, the number of potential host galaxies increases rapidly with the localization volume, which makes H_0 inference computationally demanding. Therefore, our decision to analyze events with higher SNR values helps to keep the computations manageable. While accounting for EM selection effects could allow for smaller SNR thresholds, we opted for this approach for simplicity. Moreover, events with higher SNR are the most informative, making it sufficient to analyze only this case.

We generate a signal using the SEOBNRv5PHM waveform model and analyze it using the IMRPhenomXPHM model. These waveform models are the two state-of-the-art quasi-circular spin-precessing models incorporating higher-order harmonics and used in the analysis of GW observations by the LVC Collaboration. We employ the Fisher matrix method to approximate the posterior distribution using a multivariate Normal distribution to estimate measurement accuracies of a binary's parameters. We use the publicly available Fisher matrix code GWBENCH for this purpose. Furthermore, we utilize the linear signal approximation to calculate the biases in parameter estimation resulting from the differences between the signal model and template model. For this calculation, we implement the methodology of Dhani *et al.* [33] for a more faithful representation of the systematic biases in parameter estimation.

In Table I, we report the MAP value and 90% HPD interval for μ and σ for the different detector networks and various fractions of the high-mass spin-precessing population. We quote the median values across 100 realizations to obtain a noise- and realization-averaged estimate. In the absence of systematic biases, the HPD interval for μ

TABLE I. The MAP value and the 90% HPD interval for the hyperparameters $\{\mu, \sigma\}$ in the absence and presence of systematic biases in the different detector networks and the various fractions of the embellishments to the LVK population considered here. The values quoted are median values over 100 realizations for each case.

frac.	O5		A#		XG	
	no-bias	bias	no-bias	bias	no-bias	bias
$p(\mu)$						
0%	69.5 ^{+1.59} _{-1.33}	69.2 ^{+1.52} _{-1.47}	70.2 ^{+0.57} _{-0.45}	70.4 ^{+0.44} _{-0.47}	70.0 ^{+0.01} _{-0.02}	69.8 ^{+0.09} _{-0.09}
2%	69.6 ^{+1.24} _{-1.16}	69.0 ^{+1.51} _{-1.85}	70.1 ^{+0.50} _{-0.39}	70.4 ^{+0.56} _{-0.68}	70.0 ^{+0.01} _{-0.02}	69.7 ^{+0.11} _{-0.11}
5%	69.7 ^{+1.01} _{-1.08}	68.8 ^{+1.81} _{-2.68}	70.1 ^{+0.43} _{-0.40}	69.8 ^{+0.91} _{-1.30}	70.0 ^{+0.01} _{-0.01}	69.7 ^{+0.16} _{-0.16}
10%	69.9 ^{+0.72} _{-0.65}	67.6 ^{+2.56} _{-2.83}	70.1 ^{+0.32} _{-0.29}	69.3 ^{+1.53} _{-1.53}	70.0 ^{+0.01} _{-0.01}	69.6 ^{+0.23} _{-0.24}
$p(\sigma)$						
0%	0.0 ^{+2.87} _{-0.00}	0.0 ^{+3.53} _{-0.00}	0.0 ^{+0.81} _{-0.00}	0.0 ^{+0.74} _{-0.00}	0.0 ^{+0.05} _{-0.00}	1.1 ^{+0.09} _{-0.07}
2%	0.1 ^{+2.40} _{-0.10}	1.8 ^{+2.79} _{-1.85}	0.0 ^{+0.80} _{-0.00}	0.4 ^{+0.97} _{-0.40}	0.0 ^{+0.05} _{-0.00}	1.4 ^{+0.15} _{-0.12}
5%	0.0 ^{+2.14} _{-0.00}	3.8 ^{+2.75} _{-2.12}	0.0 ^{+0.77} _{-0.00}	2.3 ^{+1.76} _{-0.86}	0.0 ^{+0.04} _{-0.00}	2.1 ^{+0.18} _{-0.13}
10%	0.0 ^{+1.58} _{-0.00}	5.0 ^{+2.18} _{-2.00}	0.2 ^{+0.46} _{-0.20}	4.4 ^{+2.24} _{-1.54}	0.0 ^{+0.04} _{-0.00}	3.0 ^{+0.39} _{-0.22}

always encompasses the injected value and σ is always consistent with zero for all the cases, validating our expectation that in an unbiased measurement the scatter of the individual posteriors is consistent with the noise distribution. In addition, we find that H_0 can be measured at $\sim 3 - 4\%$ precision with O5 depending on the fraction of the high-mass spin-precessing population. However, we see that even a 5% contamination with the high-mass spin-precessing population can cause the σ measurement to exclude zero at 90% credibility in the O5 and A# networks. Interestingly, we find that μ is consistent with the injected value for all cases in O5 and A# networks with the bias in XG at a sub-percent level. This is partially due to the fact that the uncertainty in μ is larger in the presence of systematic biases, signifying that the population hypermodel is able to absorb some of the variation due to systematic biases. This is another advantage of our approach. By contrast, we would expect the joint H_0 posterior obtained using the inaccurate model but without the hyper distribution for H_0 to be inconsistent with the injected value for such cases. Directly verifying this is difficult in practice because one encounters individual event posteriors for which the support does not overlap at machine precision, as described earlier.

Even within the hypermodel framework, the posterior on μ will tend to a delta function as the number of events increases. A more useful summary of the results is provided by the posterior predictive hyperdistribution (PPHD) (see Appendix D for the definition). Since H_0 is a constant, in the absence of systematic biases the PPHD will approach a delta function as the number of observations increases, just like the posterior on μ . However, when systematic biases are present, it

will converge to a distribution of finite width, the latter determined by the fitted variance of the population hypermodel. If at least some of the observations are free from systematic biases — which should be the case — the PPHD will encompass the true value.

Discussion— In this letter, we investigated the impact of systematic biases on the inference of H_0 due to inaccurate waveform models. We explored the galaxy catalog method to infer H_0 for a BBH population with both planned and future ground-based detector networks. In the absence of coincident EM observations, which seem to be rare, dark-siren methods offer the best prospect for standard-siren cosmology. With the many tensions in the measurements of cosmological parameters and the increasing evidence for dynamical dark energy, alternative and independent measurements are crucial to build consensus and eliminate the possibility of systematic errors in any given observation.

In addition to the putative population of BBH mergers observed by the LVK Collaboration, we studied the impact of a high-mass spin-precessing subpopulation on the H_0 estimate. Such a population is of astrophysical importance because they are a generic predictions of hierarchical mergers, as well as many population synthesis models. Furthermore, there are some hints of the existence of such a subpopulation in the GWTC-3 catalog, though more observations are needed to infer their properties. Its importance in H_0 inference is due to the difficulties in modelling such binaries and, therefore, the larger systematic biases associated with such mergers.

We used a different method to detect systematic biases in the inference of H_0 , based on testing the consistency of the variance in the distribution of the individual posteriors with the individual measurement errors to identify systematic biases. We found that this additional diagnostic is powerful in identifying the presence of systematic biases in a population inference which is otherwise not achievable. Furthermore, we reported that a small high-mass, spin-precessing subpopulation can be a dominant source of systematic bias even in O5 and A#. The effect of systematic biases is even more pronounced for XG, with H_0 estimates from even the GWTC-3 population affected by systematic biases. Our results exemplify the need for more accurate waveform models for a bright and systematics-free future.

The main limitation of our study is the reliance on the linear-signal approximation to model the impact of biases. Although this method is the most practical way to conduct our study and allows us to efficiently analyze thousands of signals spanning the entire parameter space of the BBH population, we need to better quantify its validity throughout that parameter space. In the future, we plan to use modern, machine learning based, data analysis tools, such as DINGO [51], that allow for rapid evaluation of the posteriors. Furthermore, our use of two approximate waveform models means that we cannot determine the direction of biases in a real GW event; we can only highlight the shortcomings of the current

models relative to each other. We note, however, that the methodology used here is generic and does not rely on knowing the true GW signal model. Finally, we have only considered a Gaussian model for the fitted population hyper-distribution and alternatives could also be considered. However, due to the Central Limit Theorem, we expect that the impact of any kind of systematic will

be approximately normally distributed in the limit of a large number of observations, so the approach used here should be broadly applicable.

Acknowledgements—The authors are grateful for computational resources provided by the LIGO Laboratory which National Science Foundation Grants PHY-0757058 and PHY-0823459 support.

-
- [1] B. P. Abbott *et al.* (LIGO Scientific, Virgo, 1M2H, Dark Energy Camera GW-E, DES, DLT40, Las Cumbres Observatory, VINROUGE, MASTER), A gravitational-wave standard siren measurement of the Hubble constant, *Nature* **551**, 85 (2017), [arXiv:1710.05835 \[astro-ph.CO\]](#).
 - [2] R. Abbott *et al.* (LIGO Scientific, Virgo, KAGRA), Constraints on the Cosmic Expansion History from GWTC-3, *Astrophys. J.* **949**, 76 (2023), [arXiv:2111.03604 \[astro-ph.CO\]](#).
 - [3] B. F. Schutz, Determining the Hubble constant from gravitational wave observations, *Nature (London)* **323**, 310 (1986).
 - [4] M. Fishbach *et al.* (LIGO Scientific, Virgo), A Standard Siren Measurement of the Hubble Constant from GW170817 without the Electromagnetic Counterpart, *Astrophys. J. Lett.* **871**, L13 (2019), [arXiv:1807.05667 \[astro-ph.CO\]](#).
 - [5] W. Del Pozzo, Inference of the cosmological parameters from gravitational waves: application to second generation interferometers, *Phys. Rev. D* **86**, 043011 (2012), [arXiv:1108.1317 \[astro-ph.CO\]](#).
 - [6] S. Borhanian, A. Dhani, A. Gupta, K. G. Arun, and B. S. Sathyaprakash, Dark Sirens to Resolve the Hubble–Lemaître Tension, *Astrophys. J. Lett.* **905**, L28 (2020), [arXiv:2007.02883 \[astro-ph.CO\]](#).
 - [7] S. Mukherjee, B. D. Wandelt, S. M. Nissanke, and A. Silvestri, Accurate precision cosmology with redshift unknown gravitational wave sources, *Phys. Rev. D* **103**, 043520 (2021).
 - [8] S. Mukherjee, A. Krolewski, B. D. Wandelt, and J. Silk, Cross-correlating dark sirens and galaxies: constraints on H_0 from GWTC-3 of LIGO-Virgo-KAGRA, *Astrophys. J.* **975**, 189 (2024), [arXiv:2203.03643 \[astro-ph.CO\]](#).
 - [9] D. F. Chernoff and L. S. Finn, Gravitational radiation, inspiraling binaries, and cosmology, *Astrophys. J. Lett.* **411**, L5 (1993), [arXiv:gr-qc/9304020](#).
 - [10] S. R. Taylor and J. R. Gair, Cosmology with the lights off: standard sirens in the Einstein Telescope era, *Phys. Rev. D* **86**, 023502 (2012), [arXiv:1204.6739 \[astro-ph.CO\]](#).
 - [11] W. M. Farr, M. Fishbach, J. Ye, and D. Holz, A Future Percent-Level Measurement of the Hubble Expansion at Redshift 0.8 With Advanced LIGO, *Astrophys. J. Lett.* **883**, L42 (2019), [arXiv:1908.09084 \[astro-ph.CO\]](#).
 - [12] J. M. Ezquiaga and D. E. Holz, Spectral Sirens: Cosmology from the Full Mass Distribution of Compact Binaries, *Phys. Rev. Lett.* **129**, 061102 (2022), [arXiv:2202.08240 \[astro-ph.CO\]](#).
 - [13] H. Tong, M. Fishbach, and E. Thrane, Spinning Spectral Sirens: Robust Cosmological Measurement Using Mass–Spin Correlations in the Binary Black Hole Population, *Astrophys. J.* **985**, 220 (2025), [arXiv:2502.10780 \[astro-ph.CO\]](#).
 - [14] B. Cousins, K. Schumacher, A. K.-W. Chung, C. Talbot, T. Callister, D. E. Holz, and N. Yunes, The Stochastic Siren: Astrophysical Gravitational-Wave Background Measurements of the Hubble Constant, (2025), [arXiv:2503.01997 \[astro-ph.CO\]](#).
 - [15] C. Messenger and J. Read, Measuring a cosmological distance-redshift relationship using only gravitational wave observations of binary neutron star coalescences, *Phys. Rev. Lett.* **108**, 091101 (2012), [arXiv:1107.5725 \[gr-qc\]](#).
 - [16] C. Messenger, K. Takami, S. Gossan, L. Rezzolla, and B. S. Sathyaprakash, Source Redshifts from Gravitational-Wave Observations of Binary Neutron Star Mergers, *Phys. Rev. X* **4**, 041004 (2014), [arXiv:1312.1862 \[gr-qc\]](#).
 - [17] T. G. F. Li, W. Del Pozzo, and C. Messenger, Measuring the redshift of standard sirens using the neutron star deformability, in *13th Marcel Grossmann Meeting on Recent Developments in Theoretical and Experimental General Relativity, Astrophysics, and Relativistic Field Theories* (2015) pp. 2019–2021, [arXiv:1303.0855 \[gr-qc\]](#).
 - [18] A. Dhani, S. Borhanian, A. Gupta, and B. Sathyaprakash, Cosmography with bright and Love sirens, [arXiv:2212.13183 \[gr-qc\]](#) (2022).
 - [19] J. Aasi *et al.* (LIGO Scientific), Advanced LIGO, *Class. Quant. Grav.* **32**, 074001 (2015), [arXiv:1411.4547 \[gr-qc\]](#).
 - [20] F. Acernese *et al.* (VIRGO), Advanced Virgo: a second-generation interferometric gravitational wave detector, *Class. Quant. Grav.* **32**, 024001 (2015), [arXiv:1408.3978 \[gr-qc\]](#).
 - [21] T. Akutsu *et al.* (KAGRA), Overview of KAGRA: Detector design and construction history, *PTEP* **2021**, 05A101 (2021), [arXiv:2005.05574 \[physics.ins-det\]](#).
 - [22] S. Borhanian and B. S. Sathyaprakash, Listening to the Universe with next generation ground-based gravitational-wave detectors, *Phys. Rev. D* **110**, 083040 (2024), [arXiv:2202.11048 \[gr-qc\]](#).
 - [23] D. Reitze *et al.*, Cosmic Explorer: The U.S. Contribution to Gravitational-Wave Astronomy beyond LIGO, *Bull. Am. Astron. Soc.* **51**, 035 (2019), [arXiv:1907.04833 \[astro-ph.IM\]](#).
 - [24] M. Evans *et al.*, A Horizon Study for Cosmic Explorer: Science, Observatories, and Community, [arXiv:2109.09882 \[astro-ph.IM\]](#) (2021).
 - [25] V. Srivastava, D. Davis, K. Kuns, P. Landry, S. Ballmer, M. Evans, E. D. Hall, J. Read, and B. S. Sathyaprakash, Science-driven Tunable Design of Cosmic Explorer Detectors, *Astrophys. J.* **931**, 22 (2022), [arXiv:2201.10668 \[gr-qc\]](#).
 - [26] M. Punturo *et al.*, The Einstein Telescope: A third-generation gravitational wave observatory, *Class. Quant.*

- Grav.* **27**, 194002 (2010).
- [27] M. Maggiore *et al.*, Science Case for the Einstein Telescope, *JCAP* **03**, 050, [arXiv:1912.02622 \[astro-ph.CO\]](#).
 - [28] M. Branchesi *et al.*, Science with the Einstein Telescope: a comparison of different designs, *JCAP* **07**, 068, [arXiv:2303.15923 \[gr-qc\]](#).
 - [29] N. Muttoni, D. Laghi, N. Tamanini, S. Marsat, and D. Izquierdo-Villalba, Dark siren cosmology with binary black holes in the era of third-generation gravitational wave detectors, *Phys. Rev. D* **108**, 043543 (2023), [arXiv:2303.10693 \[astro-ph.CO\]](#).
 - [30] N. Aghanim *et al.* (Planck), Planck 2018 results. VI. Cosmological parameters, *Astron. Astrophys.* **641**, A6 (2020), [Erratum: *Astron. Astrophys.* 652, C4 (2021)], [arXiv:1807.06209 \[astro-ph.CO\]](#).
 - [31] A. G. Riess *et al.*, A Comprehensive Measurement of the Local Value of the Hubble Constant with $1 \text{ km s}^{-1} \text{ Mpc}^{-1}$ Uncertainty from the Hubble Space Telescope and the SH0ES Team, *Astrophys. J. Lett.* **934**, L7 (2022), [arXiv:2112.04510 \[astro-ph.CO\]](#).
 - [32] C. B. Owen, C.-J. Haster, S. Perkins, N. J. Cornish, and N. Yunes, Waveform accuracy and systematic uncertainties in current gravitational wave observations, *Phys. Rev. D* **108**, 044018 (2023), [arXiv:2301.11941 \[gr-qc\]](#).
 - [33] A. Dhani, S. Völkel, A. Buonanno, H. Estelles, J. Gair, H. P. Pfeiffer, L. Pompili, and A. Toubiana, Systematic Biases in Estimating the Properties of Black Holes Due to Inaccurate Gravitational-Wave Models, (2024), [arXiv:2404.05811 \[gr-qc\]](#).
 - [34] V. Kapil, L. Reali, R. Cotesta, and E. Berti, Systematic bias from waveform modeling for binary black hole populations in next-generation gravitational wave detectors, *Phys. Rev. D* **109**, 104043 (2024), [arXiv:2404.00090 \[gr-qc\]](#).
 - [35] M. Pürrer and C.-J. Haster, Gravitational waveform accuracy requirements for future ground-based detectors, *Phys. Rev. Res.* **2**, 023151 (2020), [arXiv:1912.10055 \[gr-qc\]](#).
 - [36] B. P. Abbott *et al.* (LIGO Scientific, Virgo), GW170817: Observation of Gravitational Waves from a Binary Neutron Star Inspiral, *Phys. Rev. Lett.* **119**, 161101 (2017), [arXiv:1710.05832 \[gr-qc\]](#).
 - [37] A. G. Hanselman, A. Vijaykumar, M. Fishbach, and D. E. Holz, Gravitational-wave Dark Siren Cosmology Systematics from Galaxy Weighting, *Astrophys. J.* **979**, 9 (2025), [arXiv:2405.14818 \[astro-ph.CO\]](#).
 - [38] R. Abbott *et al.* (KAGRA, VIRGO, LIGO Scientific), Population of Merging Compact Binaries Inferred Using Gravitational Waves through GWTC-3, *Phys. Rev. X* **13**, 011048 (2023), [arXiv:2111.03634 \[astro-ph.HE\]](#).
 - [39] R. Abbott *et al.* (LIGO Scientific, Virgo), GW190521: A Binary Black Hole Merger with a Total Mass of $150 M_{\odot}$, *Phys. Rev. Lett.* **125**, 101102 (2020), [arXiv:2009.01075 \[gr-qc\]](#).
 - [40] R. Abbott *et al.* (KAGRA, VIRGO, LIGO Scientific), GWTC-3: Compact Binary Coalescences Observed by LIGO and Virgo during the Second Part of the Third Observing Run, *Phys. Rev. X* **13**, 041039 (2023), [arXiv:2111.03606 \[gr-qc\]](#).
 - [41] S. Rinaldi, W. Del Pozzo, M. Mapelli, A. Lorenzo-Medina, and T. Dent, Evidence of evolution of the black hole mass function with redshift, *Astron. Astrophys.* **684**, A204 (2024), [arXiv:2310.03074 \[astro-ph.HE\]](#).
 - [42] M. Lalleman, K. Turbang, T. Callister, and N. van Re-mortel, No evidence that the binary black hole mass distribution evolves with redshift, (2025), [arXiv:2501.10295 \[astro-ph.HE\]](#).
 - [43] J. S. Vink, E. R. Higgins, A. A. C. Sander, and G. N. Sabhahit, Maximum black hole mass across cosmic time, *Mon. Not. Roy. Astron. Soc.* **504**, 146 (2021), [arXiv:2010.11730 \[astro-ph.HE\]](#).
 - [44] N. C. Weatherford, G. Fragione, K. Kremer, S. Chatterjee, C. S. Ye, C. L. Rodriguez, and F. A. Rasio, Black Hole Mergers from Star Clusters with Top-Heavy Initial Mass Functions, *Astrophys. J. Lett.* **907**, L25 (2021), [arXiv:2101.02217 \[astro-ph.GA\]](#).
 - [45] M. Zevin, S. S. Bavera, C. P. L. Berry, V. Kalogera, T. Fragos, P. Marchant, C. L. Rodriguez, F. Antonini, D. E. Holz, and C. Pankow, One Channel to Rule Them All? Constraining the Origins of Binary Black Holes Using Multiple Formation Pathways, *Astrophys. J.* **910**, 152 (2021), [arXiv:2011.10057 \[astro-ph.HE\]](#).
 - [46] S. S. Bavera, M. Fishbach, M. Zevin, E. Zapartas, and T. Fragos, The $\chi_{\text{eff}} - z$ correlation of field binary black hole mergers and how 3G gravitational-wave detectors can constrain it, *Astron. Astrophys.* **665**, A59 (2022), [arXiv:2204.02619 \[astro-ph.HE\]](#).
 - [47] S. Biscoveanu, T. A. Callister, C.-J. Haster, K. K. Y. Ng, S. Vitale, and W. M. Farr, The Binary Black Hole Spin Distribution Likely Broadens with Redshift, *Astrophys. J. Lett.* **932**, L19 (2022), [arXiv:2204.01578 \[astro-ph.HE\]](#).
 - [48] C. S. Ye and M. Fishbach, The Redshift Evolution of the Binary Black Hole Mass Distribution from Dense Star Clusters, *Astrophys. J.* **967**, 62 (2024), [arXiv:2402.12444 \[astro-ph.HE\]](#).
 - [49] J. R. Gair and C. J. Moore, Quantifying and mitigating bias in inference on gravitational wave source populations, *Phys. Rev. D* **91**, 124062 (2015), [arXiv:1504.02767 \[gr-qc\]](#).
 - [50] M. Isi, W. M. Farr, and K. Chatziioannou, Comparing Bayes factors and hierarchical inference for testing general relativity with gravitational waves, *Phys. Rev. D* **106**, 024048 (2022), [arXiv:2204.10742 \[gr-qc\]](#).
 - [51] M. Dax, S. R. Green, J. Gair, M. Pürrer, J. Wildberger, J. H. Macke, A. Buonanno, and B. Schölkopf, Neural Importance Sampling for Rapid and Reliable Gravitational-Wave Inference, *Physical Review Letters* **130**, 171403 (2022), [arXiv:2210.05686 \[gr-qc\]](#).

SUPPLEMENTARY MATERIALS

Appendix A: MICECAT

We assign GW sources to galaxies taken from MICECAT, the Grand Challenge. It is a mock galaxy catalog that covers one octant of the sky up to a redshift of 1.4. While the full catalog contains ~ 205 M galaxies, we only consider galaxies with luminosity $L > 10^{10} L_\odot$, where L_\odot is the solar luminosity, as possible hosts reducing the catalog size to ~ 83 M galaxies. The H_0 calculation is done using this reduced catalog for consistency. The fiducial cosmological model in MICECAT is a flat Λ CDM model with parameters $H_0 = 70 \text{ km s}^{-1} \text{ Mpc}^{-1}$ and $\Omega_m = 0.25$. We choose the same model for simulating GW sources.

Appendix B: GW population

With close to 100 observations, we have an understanding of how the binary merger population is distributed. We simulate two populations of BBH mergers with 100k binaries in each. All parameters are the same across both the populations except the masses and spins. The host galaxy for each merger is assigned by randomly drawing galaxies from MICECAT. This specifies the redshift distribution and sky positions of the two populations. Since the MICECAT mock catalog covers only one-octant of the sky the simulated GW sources are also restricted to this single octant in the sky. We will always consider GW networks with at least 3 non-colocated detectors and, therefore, we expect each octant in the sky to give similar results since the network sensitivity for tensor polarizations does not vary much across the sky. A binary orbit is assumed to be randomly oriented, and the polarization angle and orbital phase are also chosen randomly. The time of coalescence is fixed to some fiducial value.

In the first population, the masses and spins are chosen to follow **Power Law + Peak** and **DEFAULT** distributions of GWTC-3, respectively. The motivation for the second population, denoted “high-mass spin-precessing”, is to study the impact of an yet unobserved subpopulation consisting of binaries with large masses, large mass ratios, and large precessing spins. The impact of such a subpopulation on the astrophysical and cosmological inference using GWs is of interest to the waveform modelling community because it lies in a region of the parameter space that is relatively poorly modelled. On the astrophysical side, such a population is of interest because the hierarchical merger scenario can produce them. We sample uniformly in the total source-frame mass and the inverse mass ratio in the interval $[10, 200]M_\odot$ and $[1, 30]$, respectively, and place a constraint that the smaller mass is always greater than $5M_\odot$. This results in a non-uniform distribution of the two masses with a preference for larger masses. The spin magnitudes are sampled from a uniform distribution spanning its domain and the spin angles are isotropically distributed. Subsequently, this sample is

subsampled such that the χ_p distribution is uniform.

The final simulated populations are linear combinations of these two underlying populations with varying relative weights. The distributions of the total mass, mass ratio, and spin-precession parameter are shown in Fig. 3.

Appendix C: H_0 inference

Consider a set of N_{obs} events with single event parameters $\{\boldsymbol{\theta}_i\}_{i=1}^{N_{obs}}$ and data $\mathcal{D} = \{\mathcal{D}_{GW}^i, \mathcal{D}_{EM}^i\}_{i=1}^{N_{obs}}$. The EM data, consisting of the mock galaxy catalog MICECAT, contains the redshift, position in the sky, and luminosity of all galaxies in the catalog. While one expects the hosting probability to depend on galaxy properties like its luminosity or star formation rate, GW observations do not provide a clear answer yet. For quasi-circular, spin-precessing systems considered here, the GW data depends on the usual 15 parameters: component masses, component spins, location, orientation, and phase. In general, one expects the mass and spin distributions to evolve with redshift and, therefore, encode information about the true cosmology. However, current GW observations are uncertain of the form of such a dependence. Even in the absence of a redshift evolution of the mass distribution, the deviation in the observed detector-frame mass distribution from the source-frame mass distribution encodes the redshift, a method that exploits this is known as *spectral siren* [9, 10]. Nevertheless, since we are interested in investigating H_0 systematics while using the galaxy catalog method, it is beneficial to marginalize over all the intrinsic parameters to isolate the effect of the galaxy catalog. We are, in effect, using less information than what is available to us and this results in the H_0 posteriors being marginally broader than what they could be.

The contribution of a single event to the likelihood of H_0 , after marginalisation of the joint likelihood over the number of detections using a log-uniform prior, is given by

$$\mathcal{L}(\mathcal{D}_{GW}^i, \mathcal{D}_{EM}^i | H_0) = \frac{1}{\beta(H_0)} \times \int dz d\Theta \mathcal{L}_{GW}(\mathcal{D}_{GW}^i | d_L(z, H_0), \Theta) p(z, \Theta), \quad (\text{C1})$$

where d_L and Θ are the luminosity distance and sky position, respectively, $\mathcal{L}_{GW}(\cdot)$ is the GW likelihood, marginalized over all other parameters, and $p(z, \Theta)$ is the joint probability distribution for the redshift and sky position of GW sources obtained from the galaxy catalog. The denominator, $\beta(H_0)$, is a normalization constant given by,

$$\beta(H_0) = \int d\mathcal{D}_{GW}^i dz d\Theta \mathcal{L}_{GW}(\mathcal{D}_{GW}^i | d_L(z, H_0), \Theta) p(z, \Theta), \quad (\text{C2})$$

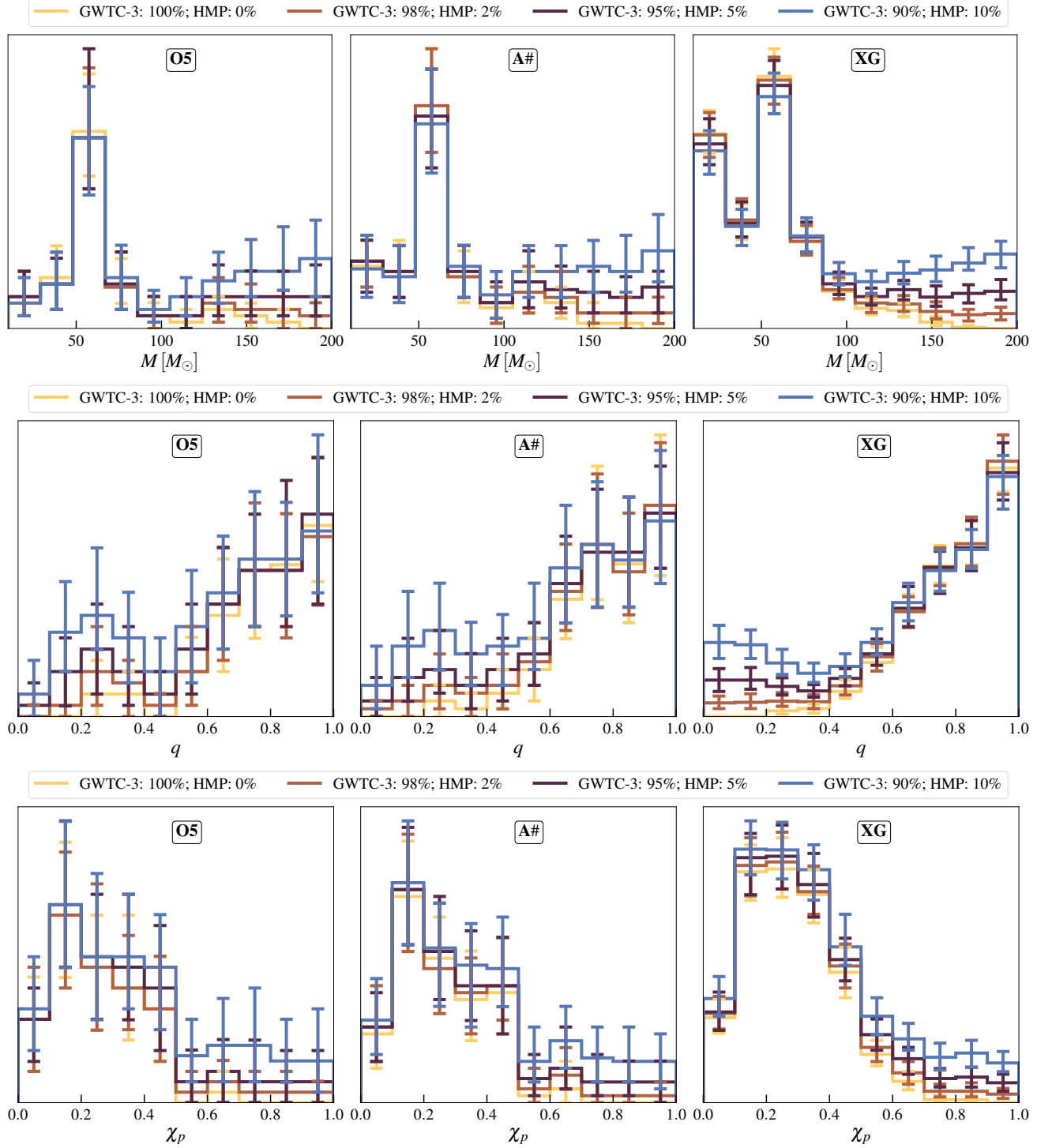


FIG. 3. Mixture population crossing SNR threshold

where the \mathcal{D}_{GW}^i integration is over all data that is above the detection criteria. This term corrects for selection effects. Here, we have assumed that the detection criteria is based on the GW data alone and the galaxy catalog is complete.

We simplify Eq. (C1) by assuming that the sky location

and luminosity distance separate in the GW likelihood and the redshift prior. The GW likelihood then becomes $\mathcal{L}_{GW}(\mathcal{D}_{GW}^i | d_L(z, H_0), \Theta) = p(\hat{d}_L^i | d_L(z, H_0))p(\hat{\Theta}^i | \Theta)$ where \hat{d}_L^i and $\hat{\Theta}^i$ are the observed luminosity distance and sky location of a GW event. We simulate an observed value by drawing a point-estimate from a Normal

distribution centred at the injected value and covariance given by the inverse of the Fisher matrix. Furthermore, we regard the EM sky positions to be precise and set these to δ -functions. Under these assumptions, Eq. (C1) becomes

$$\mathcal{L}(\mathcal{D}^i|H_0) = \frac{1}{\beta(H_0)} \sum_{j=1}^{N_{gal}} \int dz_j \mathcal{N}(\hat{d}_L^i | d_L(z_j, H_0)) w_j^i p(z_j) \quad (\text{C3})$$

where $w_j^i = \mathcal{N}(\hat{\theta}^i | \theta_0^j, \Sigma^i)$ with θ_0^j the position of the j -th galaxy in the galaxy catalog and N_{gal} the total number of galaxies in the localization volume. $p(z_j)$ is the posterior distribution on the redshift. We assume the redshifts to be known precisely and model it as a δ -function. This is a reasonable assumption if spectroscopic measurements of the redshifts of the galaxies are available. On the contrary, photometric measurements have larger measurement errors which would need to be taken into account.

Appendix D: Population diagnostic

The posterior distribution on the hyperparameters μ, σ is given by

$$p(\mu, \sigma | \{\mathcal{D}\}) = p(\mu, \sigma) \prod_{i=1}^{N_{obs}} \int dH_0^i \mathcal{L}(\mathcal{D}^i | H_0^i) \mathcal{N}(H_0^i | \mu, \sigma) \quad (\text{D1})$$

where the H_0 likelihood is defined in Eq. (C3). We define the PPHD on H_0 as

$$p(H_0 | \{\mathcal{D}\}) = \int d\mu d\sigma \mathcal{N}(H_0 | \mu, \sigma) p(\mu, \sigma | \{\mathcal{D}\}). \quad (\text{D2})$$

Appendix E: PPHD

In Fig. 4, we show the PPHD for the GWTC-3 population in XG network. The distribution tends towards a δ -function in the absence of systematic biases but asymptotes to a finitely wide distribution otherwise.

In Fig. 5, we show the joint H_0 posterior (which is the μ posterior conditioned on $\sigma = 0$), the marginalised μ posterior and the PPHD for the real events analyzed in the GWTC-3 cosmology paper [2].

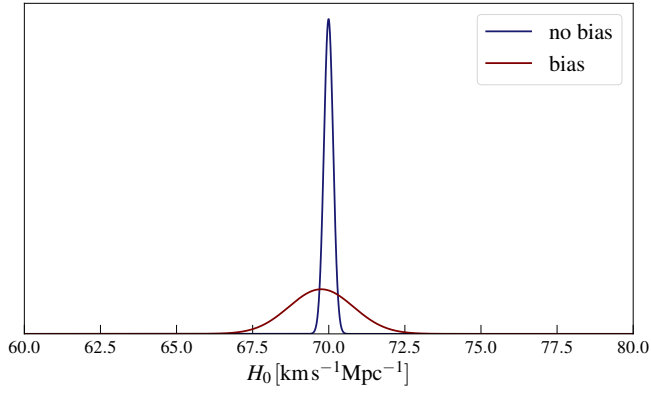


FIG. 4. The posterior predictive distributions (PPD) of the population parameter H_0 for a GWTC-3 population in the XG network. The PPD, in the absence of systematic biases, tends toward a δ -function, as expected. On the other hand, a non-zero σ causes the PPD to have a finite width, as in the presence of systematic biases.

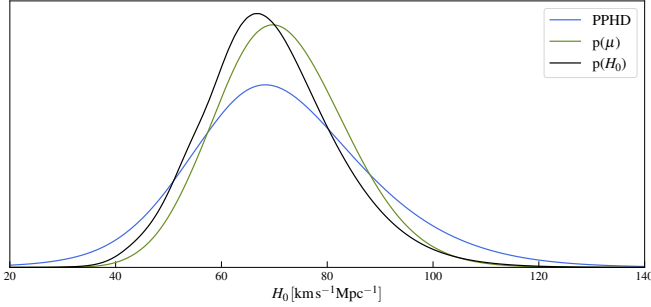


FIG. 5. The posterior predictive distribution, the marginalized μ distribution, and the joint posterior distribution on H_0 obtained from the events used in the GWTC-3 cosmology paper [2]. We do not see any indication of systematic biases. Note that even though the μ posterior is very similar to the joint H_0 posterior but we are not yet in the large number of observations limit where the two will coincide.